Optimization and Surrogate Modeling of Tip-Rake Propellers

Andreas Arapakopoulos[1], Claus Abt[1], Simon Hauschulz[1], Stefan Harries[1]

[1]FRIENDSHIP SYSTEMS AG, Potsdam, Germany

ABSTRACT

This paper introduces a novel tool designed for the efficient development of unconventional propellers, notably tip rake and highly skewed propellers. The initial phase involves a parametric model that accepts any conventional propeller as input, transforming it into an unconventional one. This model introduces parameters that influence the geometry of the blade either globally or locally at the tip. The numerical analysis is conducted with *panMARE*, a *BEM* code from *TUHH*, under open water conditions. The validation of *panMARE* is accomplished by comparing it with the derived polynomials from B-series experimental results. Based on four main inputs: propeller diameter, inflow velocity, advance coefficient and required thrust coefficient an optimal 5-bladed B-series propeller is identified via cavitation examination using the Burrill diagram. This leads to a single-objective optimization process that utilizes the aforementioned parametric model. The process aims to maximize efficiency of the propeller with targeted thrust and a constraint on cavitation. Finally, the various outcomes from the optimization across different operational conditions are used for the development of a surrogate model for immediate result retrieval, introducing a promising new design approach based on artificial intelligence (AI).

Keywords

Unconventional Propellers, Parametric Modeling, CFD, Optimization, Surrogate Model.

1 INTRODUCTION

While traditional propellers have served the maritime industry for years (Carlton 2018), the increasing demands for energy efficiency, CO_2 and noise emission reductions, as shown by Sherbaz & Wenyang (2012) have made the need for unconventional and even more efficient designs evident (Castro et al. 2019). Historically, experiments were the standard for testing such innovations (Newman 2018). Nowadays, the rise of Computational Fluid Dynamics (CFD) has provided an efficient and comprehensive approach, enabling an extensive exploration of the design space (Versteeg & Malalasekera 2007). *CFD* is fundamentally divided into two categories: inviscid and viscous flow computations (Zawawi et al. 2018). In this paper, the focus is on a Boundary Element Method (*BEM*) code from *TUHH*, named *panMARE* (Bauer & Abdel-Maksoud 2012), a well-documented platform that has proven its reliability in numerous projects (Yu et al. 2013). For generating the geometry of the propeller, the *CAD* software *CAESES* is employed (Harries 2020). This software stands out not only for its prowess in developing parametric models but also for its seamless integration capabilities with commercial simulation software and in-house codes. Furthermore, the optimization tools of *CAESES* significantly augment the scope of this research (Harries & Abt 2019). In the broader context of technology, the integration of AI and simulation-driven optimization is proving to be transformative (Harries & Abt 2019). Through the creation of a surrogate model for 5-bladed propellers (Tadros et al. 2018), this study underscores the feasibility of generating optimal design outputs from just four main parameters, namely: propeller diameter, inflow velocity, advance coefficient (alternatively, rotational speed) and required thrust coefficient. This streamlined approach allows for swift adjustments of the pitch, chord, skew and rake, the typical radial distribution functions of a marine propeller (Kerwin 1986). Navigating through this paper, Section 2 focuses on the Wageningen B-series propellers, while Section 3 offers insights into the BEM and *panMARE* code. Section 4 introduces the parametric model central to the research approach. The optimization process is detailed in Section 5, with Section 6 discussing the surrogate model approach. The paper concludes in Section 7, presenting the findings of this research.

2 WAGENINGEN B-SERIES PROPELLERS

The Wageningen B-series propellers are well known as one of the most extensive and frequently employed propeller series in marine propulsion (Oosterveld & van Oossanen 1975), initially introduced through a series of papers (Troost 1951) and later tested at the Netherlands Ship Model Basin (Van Lammeren & Vossers 1957).

2.1 Main Parameters

The B-series can be understood as a parametric model, represented by the notation $BZ - y$. Here, B signifies the B-series, Z corresponds to the number of blades ranging from 2 to 7 and y represents the expanded area ratio A_E/A_0 spanning from 0.3 to 1.05. Another crucial parameter is the face pitch-diameter ratio P/D, where D denotes diameter and P/D varies between 0.6 and 1.4. These primary parameters, complemented by secondary attributes such as rake angle and thickness at the leading and the trailing edge, collectively provide a comprehensive definition of the propeller blade.

2.2 Polynomials for k_T and k_Q

The B-series propellers were tested in uniform flow with a specified Reynolds number of $2x10\hat{}6$. The results from these tests were subjected to multiple regression analyses. Polynomial equations, as shown by Barnitsas et al. (1981) (see Equation 1) were derived to represent the thrust and the torque coefficients as functions of Z, A_E/A_0, P/D and J. For Reynolds numbers exceeding $2x10\hat{}6$, adjustments of the aforementioned coefficients should be made using correction terms $\Delta K_Q(R_n)$ and $\Delta K_T(R_n)$.

$$\begin{cases} k_{T\,pol} = \sum_{n=1}^{39} C_n(J)^{s_n} \left(\frac{P}{D}\right)^{t_n} \left(\frac{A_E}{A_0}\right)^{u_n} (Z)^{v_n} + \Delta K_T(R_n) \\ k_{Q\,pol} = \sum_{n=1}^{47} C_n(J)^{s_n} \left(\frac{P}{D}\right)^{t_n} \left(\frac{A_E}{A_0}\right)^{u_n} (Z)^{v_n} + \Delta K_Q(R_n) \end{cases} \quad (1)$$

2.3 Burrill Cavitation Diagram

The Burrill cavitation diagram is a widely acknowledged criterion for fixed-pitch conventional propellers in the preliminary design stage, assisting designers in selecting suitable conventional propellers (Burrill & Emerson 1963). Essentially, the diagram aids in predicting the percentage cavitation on the back side of the propeller blade by calculating (see Equation 2) the mean thrust load coefficient on the blades (τ_c in y-axis), as well as the cavitation number at a 0.7 radius ($\sigma_{0.7R}$ in x-axis). This is integrated inside *CAESES*, as shown in Figure 1. In Equation 2, where T represents the generated thrust from the propeller, A_P denotes the projected area of the propeller, V_A stands for the inflow velocity, n represents the rotational speed, p_0 signifies the reference pressure at sea level, ρgh corresponds to the hydrostatic pressure and p_v represents the vapor pressure (when water undergoes a phase transition from liquid to vapor).

$$\begin{cases} \tau_c = \dfrac{T}{0.5A_P\rho[V_A^2 + (0.7\pi nD)^2]} \\ \sigma_{0.7R} = \dfrac{p_0 + \rho gh - p_v}{0.5\rho[V_A^2 + (0.7\pi nD)^2]} \end{cases} \quad (2)$$

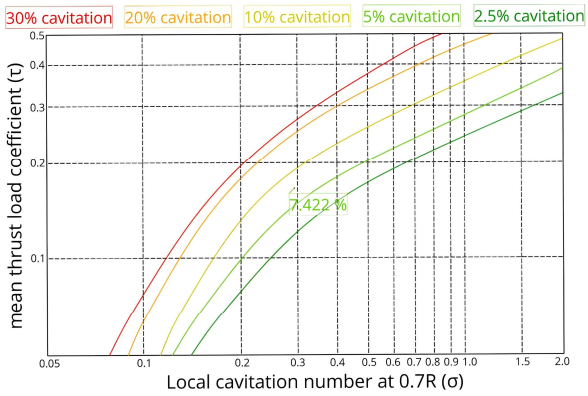

Figure 1: Burrill Diagram Integrated in CAESES

3 BEM CONFIGURATION

Potential flow theory, as introduced in (Hess & Smith 1967) describes the fluid flow around solid objects like marine propellers by omitting viscosity, thereby facilitating the expression of the fluid dynamics problem through a velocity potential and significantly reducing computational costs (Kerwin et al. 1987). Within a *BEM* framework, a panel mesh is employed to represent the body and the wake geometry (Hess 1972). Figure 2 depicts the pressure distribution on the blade, highlighting the correct wake geometry in blue, which satisfies the Kutta condition at both the trailing edge and in the wake (Crighton 1985). This offers a marked advantage over other computational techniques, such as *RANS* simulations (Xiao & Cinnella 2019), where generating a mesh for the entire computational domain can be a time-consuming task (Sosnowski et al. 2018). The pressure distribution showcased in Figure 2 is derived from potential flow theory. Based on the pressure distribution, both the thrust and the torque generated by the propeller can be determined, leading to the derivation of its associated open water characteristics, as detailed in Equation 3. The *panMARE* code used in this work incorporates a sheet cavitation model (Fine 1992). This enables the determination of the cavity area A_{cav}, locating cavitated regions on the blade. Furthermore, by calculating the cavitation thickness and its distribution, as visualized in Figure 3, the cavity volume V_{cav} can be deduced.

$$\begin{cases} k_{T\,pan} = \dfrac{T_{pan}}{\rho n^2 D^4} \\ k_{Q\,pan} = \dfrac{Q_{pan}}{\rho n^2 D^5} \end{cases} \quad (3)$$

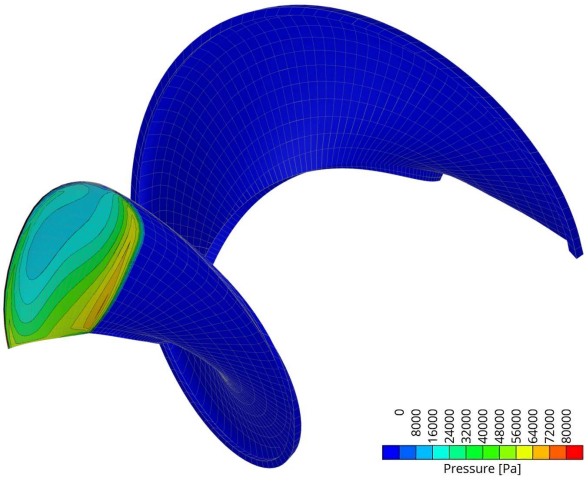

Figure 2: Pressure Distribution on Blade with Wake (blue)

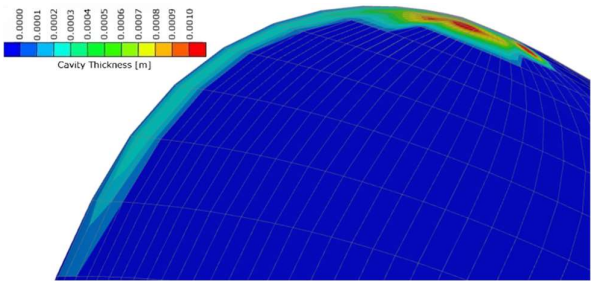

Figure 3: Cavity Thickness Distribution on Blade

3.1 Integration of CAESES with panMARE

The panel mesh geometries, along with additional information about the properties of the fluid, will function as input for the *panMARE* code (Santos et al. 2017). This input can be easily generated in the *CAESES* software, which offers dedicated tools for propeller geometries. The integration of *panMARE* code can be implemented through the *API* of *CAESES* (Netzband et al. 2018).

3.2 Validation of panMARE

A methodical comparison between *panMARE* results and B-series propellers are carried out across three different B-series propellers, as illustrated in Figure 4. The three samples are 5-bladed propellers with different A_E/A_0 ratios: 0.75, 0.60 and 0.45 and each one correspondingly is selected with different P/D ratios: 0.8, 1.0 and 1.2. Each of these propellers is subjected to be tested at five different Advance Coefficients. These J values are selected to be 0.05 units apart, with the middle value approximating the J at which peak efficiency occurs. Dashed lines in Figure 4 represent the open-water characteristics derived from B-series polynomials, while continuous lines display results from *panMARE*.

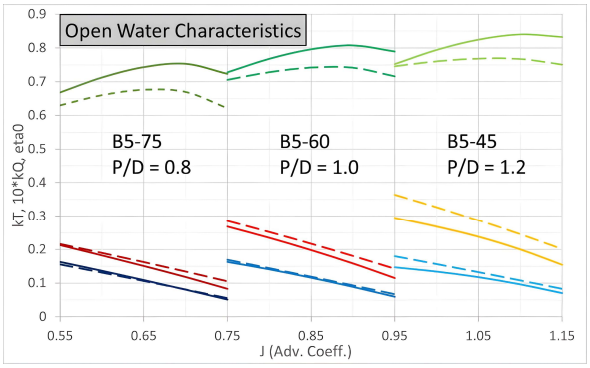

Figure 4: Comparisons of B-series Polynomials (dashed lines) and panMARE Simulations (continuous lines)

Upon closer examination of the comparison, it becomes evident that *panMARE* simulations generally yield results that closely match the thrust coefficients of the polynomials. However, across all advance ratios, the *panMARE* results consistently exhibit a slight underestimation of torque coefficients, resulting in a parallel offset. Consequently, this leads to an overestimation of propeller efficiency, although *panMARE* follows with the overall trend observed in the polynomials. This outcome is reasonable, as viscosity is not considered in *BEM*. Instead of the viscosity, a "heuristic" friction model, which relies on skin friction over a flat plate, is incorporated (Hoerner 1965). The validity of this approach is maintained by selecting advance coefficients near the peak of propeller efficiency for each case. Deviating significantly from these values would alter the angle of attack, potentially causing flow separation, a phenomenon that BEM codes cannot consistently predict.

4 PARAMETRIC MODEL

In this section attention is given to the Parametric Model for Unconventional Propellers (*PMUP*). Unlike a fully parametric model that can generate an entirely new geometry from scratch (Epps et al. 2009, Ahmed et al. 2023), *PMUP* functions as a partial parametric model (Lim et al. 2014). It requires an imported base geometry on which the design variables operate to shape the final, unconventional propeller. In the scope of this research, the parametric model is employed to transform B-series propeller designs into unconventional forms, characterized by features such as a tip rake and high skew angles.

4.1 Radial Distributions

Upon importing the base geometry, the initial focus is to identify and isolate radial functions that are fundamental to marine propellers (Mizzi, K., Demirel, Y. K., Banks, C., Turan, O., Kaklis, P., & Atlar, M. (2017).). These radial distribution functions, such as pitch, chord, skew and rake, serve as the baseline geometry for the transformations conducted in parametric model (see Figure 5). Through the adjustment of these distributions using the design variables *PMUP* (see Table 1), the model can facilitate the conversion of a conventional propeller into an unconventional one. Notably, the parameters like *modRake* and *modSkew* are instrumental in generating unconventional propellers, as *modRake* produces propellers with either forward or backward tip rake and *modSkew* results in highly skewed propeller designs.

Parameters	***Range***	***Description***
modPitchHub	$[-0.2, 0]$	Modifies pitch at the hub
modPitchTip	$[-0.2, 0]$	Modifies pitch at the tip
modChord	$[-0.1, 0.1]$	Moves the pos. of max. chord
scaleChord	$[0.9, 1.1]$	Scales the overall chord size
modRake	$[-0.15, 0.15]$	Modifies rake at the tip
rakeAngle	$[-20, 20]$	Defines the rake angle
modSkew	$[0, 0.15]$	Modifies skew at the tip
splitRadius	$[0.7, 0.9]$	Defines where *modRake* is enabled

Table 1: Parameters of PMUP

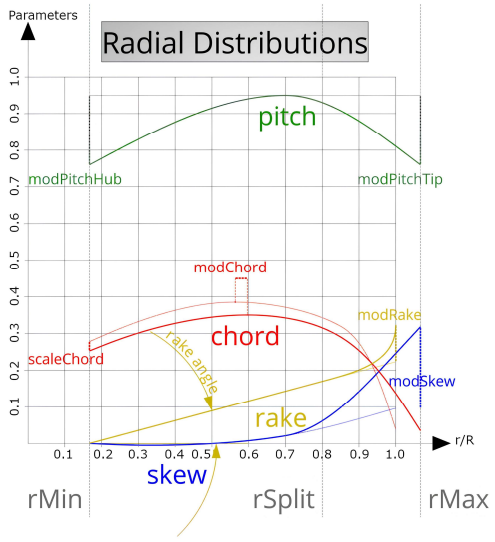

Figure 5: Design Variables of PMUP

In Figure 5, the parameter *rSplit* (*splitRadius*) is highlighted, representing the radial position from which *modRake* is enabled. Additionally, *rMax* is identified in the context of tip rake propellers. These propellers extend beyond the imported diameter (Lungu 2019), posing challenges for their representation in *.PFF* files (Krasilnikov 2019), which are the standard file format for marine propellers. For this reason, the remaining radial distribution functions, except for the tip rake, extend beyond $rR = 1$ and reach up to *rMax*.

4.2 Normalized Surfaces

In the blade generation process, two dimensionless surfaces are utilized, each scaled relative to the diameter of the propeller. The first surface, known as the profile surface, embodies the geometric info of the profile of the blade (Benini 2004), such as its maximum value and the position of the camber and the thickness. This surface starts from a non-dimensional position at the hub and extends to the tip span-wise. The chord-wise direction of this surface ranges from 0 to 1, as it does not include specifics about chord length. The second surface, referred to as the central or camber surface, serves as the zero-lift surface and is devoid of any profile information. This surface also spans from a non-dimensional position at the hub up to the tip, similar to the profile surface and encapsulates information on pitch, rake and skew distributions. By integrating information from these two dimensionless surfaces, the geometry of the blade is subsequently developed and then scaled to the propeller's diameter to restore the dimensionality (see Figure 6). Given that the B-series blades have been stress-tested, the profile surface remains undistributed, making it a safe profile selection. Consequently, the alterations of the *PMUP* are solely concentrated on the camber surface, thus avoiding an increase in the design variables of the parametric model and the expansion of the problem's dimension.

4.3 Blade Geometry

The blade requires specific attributes to serve as an input for a *BEM* code. A sharp trailing edge is crucial to ensure the Kutta condition at the trailing edge (Morino & Bernardini 2001). Interestingly, the blade does not terminate with a specialized tip geometry; instead, the corresponding thickness and chord is retained until the final cylindrical section (Politis 2004). The final geometry in *CAESES* is modeled as a *NURBS* surface (Piegl & Tiller 1996), which is then transformed into a panel mesh. This mesh comprises 30 chord-wise panels and 20 span-wise panels, a configuration determined through sensitivity analysis focusing on mesh refinement (see Figure 2 and Figure 6). Denser spacing is allocated for both the leading edge and the tip to ensure accurate simulations. In Figure *6*, three distinct blade panel meshes are illustrated: a backward tip rake (depicted in light pink on the left), a forward tip rake (shown in light green on the right) and a conventional design (highlighted in light blue at the center. This visualization aims to underscore the significance of the *modRake* parameter as it varies from its lower bound to upper bound, which plays a crucial role in the optimization process.

Figure 6: Blade Panel Meshes: Non-Tip Rake(middle) Backward & Forward Tip Rake (left & right)

5 OPTIMIZATION FRAMEWORK

Within this optimization framework, the target is to identify a 5-bladed optimal propeller design by exploring both conventional and unconventional designs via the parametric propeller model. The optimization process is conducted in two stages. The initial stage bypasses simulations, relying on the polynomial outcomes from the B-series and the back cavitation predictions from the Burrill diagram. This stage sets the groundwork for the subsequent stage, where the resulting geometry from the first stage serves as the baseline design for subsequent explorations on unconventional propeller designs.

5.1 B-series Setup

The first stage only uses the B-series polynomials and the back cavitation estimations from the Burrill diagram. lists the optimization inputs, with a focus on 5-bladed propellers. Although the B-series encompasses propellers ranging from 2 to 7 blades, a 5-blade design is preferred due to its contemporary relevance in commercial ship design. Additionally, Table 2 highlights the input ranges, with the diameter of the propeller and the inflow velocity restricted to a narrow bracket, primarily targeting cargo ships for commercial use. This conservative approach is taken because the tool is in its early stages of development, allowing for a step-by-step progression. Choosing the advance coefficient and the required thrust coefficient instead of rate of revolution and the required thrust as inputs offers the advantage of dimensionless inputs, precluding unrealistic values by users. Equation 4 and Equation 6 facilitate direct computations for the rotation rate and the required thrust respectively. Meanwhile, the projected area (see Equation 5), required as an input for the Burrill diagram (see Equation 9) is a semi-empirical

formula tailored for conventional propellers. The projected area of the blade is needed for Equation 2 for calculating the mean thrust load coefficient. On the other hand, Equation 6 is standard within the field of propulsion (Gerr 1989).

$$n = \frac{V_A}{JD} \tag{4}$$

$$A_P = (A_E/A_0)\pi(0.5D)^2(1.067 - 0.229\,P/D) \tag{5}$$

$$T_{req} = k_{T_{req}}\rho n^2 D^4 \tag{6}$$

Inputs	*Range*	*Units*	*Description*
D	[6,8]	meters	Diameter of the Prop.
V_A	$[18, 22]$	knots	Inflow Velocity
J	$[0.45, 1.25]$	-	Advance Coefficient
$k_{T_{req}}$	$[0.05, 0.2]$	-	Req. Thrust Coefficient
Z	5	-	Number of Blades

Table 2: Main Inputs in the Optimization Framework

As previously discussed, the B-series polynomials enable the computation of open water characteristics, as illustrated in Figure 4. When inputs from Table 2 are applied, the thrust can be derived from Equation 7, while the propeller efficiency is determined using Equation 8. This propeller efficiency serves as the objective function of the optimization and the goal is to maximize it.

$$T_{pol} = k_{T_{pol}}\left(J, \frac{P}{D}, \frac{A_E}{A_0}, Z, R_n\right)\rho n^2 D^4 \tag{7}$$

$$max\,\eta_{0_{pol}} = max\frac{Jk_{T_{pol}}\left(J, \frac{P}{D}, \frac{A_E}{A_0}, Z, R_n\right)}{2\pi k_{Q_{pol}}\left(J, \frac{P}{D}, \frac{A_E}{A_0}, Z, R_n\right)} \tag{8}$$

The unknown variables in Equation 8 encompass the pitch-diameter ratio P/D and the expanded area ratio A_E/A_0. For the optimization, the Tangent Search Method (*TSearch*) is employed. This method is reputed for its reliability, especially in handling small-scale, single-objective optimization problems that come with inequality constraints. These constraints are twofold: they aim to restrict cavitation (see Equation 9), determined by the Burrill diagram and to achieve the proper range of the permittable thrust. Typically, designers incorporate an additional percentage to account for factors such as hull fouling and adverse weather conditions, which can augment resistance. This supplementary force can range up to 40% (Birk 2019). Given that *panMARE* tends to overestimate generated thrust, aligning the thrust values across both optimization stages is paramount, as outlined in Equation 10.

$$c = Burrill(\sigma_{0.7R}, \tau_c) < 30\% \tag{9}$$

$$T_{req} \leq T_{pol} \leq 1.3T_{req} \tag{10}$$

TSearch is a gradient-free local optimization algorithm, see for instance (Papakonstantinou et al. 2019), which necessitates starting from a promising design. The design is controlled by the two aforementioned unknowns, determined as follows. For P/D, Figure 4 reveals – as confirmed by the B-series open water tests - that the best propeller efficiency for a specific J is located around $P/D = J + 0.15$. Concerning the expanded area ratio, its value is calculated using Equation 11. In general, the expanded area ratio of a blade is roughly proportional to the thrust it generates (Suen & Kouh, 1999). For the B-series, the range of A_E/A_0 values extend from a minimum of 0.3 to a maximum of 1.05. The maximum and minimum values k_T are defined by the input boundaries of the parametric model, as outlined in Table 2.

$$\frac{A_E}{A_0} = 0.3 + (1.05 - 0.3)\frac{k_{T_{req}} - k_{T_{min}}}{k_{T_{max}} - k_{T_{min}}} \tag{11}$$

5.2 Unconventional Designs Setup

The best designs produced in the initial stage serve as the starting inputs for the second phase, which also employs the *TSearch* algorithm. In this phase, the open-water characteristics of the propeller are determined using the *panMARE* code paired with the *PMUP*, enabling a more refined optimization of both conventional and unconventional designs. The design variables used in the optimization are detailed in Table 1. Notably, the *splitRadius* is preset to 0.8. A sensitivity analysis revealed that this variable had a minimal impact on results. Setting it at 0.8, a midpoint within the range of the variable, yielded consistent and reasonable outcomes. It is crucial to keep the number of variables to a minimum, ensuring a manageable design space dimensionality that can be efficiently scanned. At the same time, it is essential not to compromise on the diversity of shapes (Arapakopoulos et al. 2019). The *PMUP* aids in this balancing act by using geometrically meaningful variables, defining an appropriate design space and setting suitable constraints. In Equation 12, the objective function for this configuration is presented, which is the propeller efficiency with an aim to maximize it. The constraints for this arrangement are twofold: to limit cavitation and to achieve the targeted thrust, with values sourced from *panMARE*, as showcased in Equation 13 and Equation 14. In Equation 13 the cavity area is limited to be no more than 10% of the expanded area, which is lower than 30% chosen in the B-series setup.

$$max\,\eta_{0_{pan}} = max\frac{Jk_{T_{pan}}}{2\pi k_{Q_{pan}}} \tag{12}$$

$$A_{cav} < 0.1A_E \tag{13}$$

$$T_{req} \leq T_{pan} \leq 1.3T_{req} \tag{14}$$

5.3 Numerical Results

This sub-section presents a case study illustrating the robustness of the proposed methodology. The optimization process begins with a vector input set at the midpoint of the corresponding range:

$$\left[D, V_A, J, k_{T_{req}}, Z\right] = [7\ m, 20\ knots, 0.85, 0.125, 5]$$

The initial result from the first T-Search yields a *B5-73* propeller with $P/D = 1.032$, representing a conventional design. A conventional propeller of this type is well-suited for a variety of commercial cargo ships, including medium-sized container vessels (Man 2023). Building upon this conventional design, a second T-Search is conducted to create a tip rake propeller with a targeted thrust and a cavitation level lower than the initial design. The convergence history of the second optimization is illustrated in Figure 7. In this plot, red triangles represent design instances that violate the constraints related to the cavitation and the thrust, while green circles denote valid designs. The blue circle highlights the optimum design, which attains the highest efficiency. In valid designs, the sudden increase in propeller efficiency is primarily influenced by parameters that impact the propeller geometry at the tip, such as *modRake*, *modSkew* and *modPitchTip*. The red triangles can be categorized based on their thrust characteristics. Instances with overestimated efficiency possess higher generated thrust than desired, while those with underestimated efficiency exhibit thrust values lower than desired.

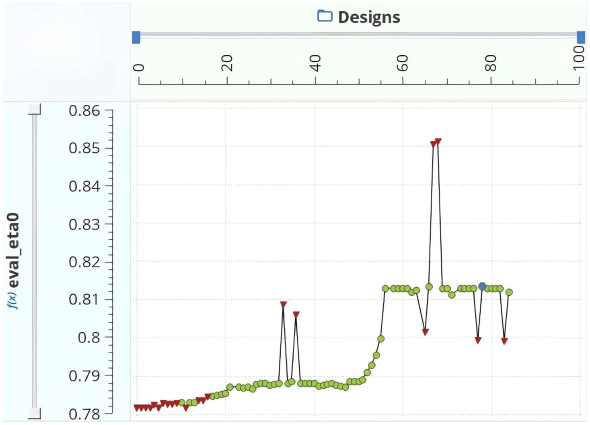

Figure 7: T-search Optimization with panMARE and PMUP

6 SURROGATE MODEL

Surrogate modeling stands as a significant milestone in modern engineering methodologies (Koziel et al. 2011). Offering simplified versions of intricate models, it enables rapid decision-making, bypassing the time-consuming set-up, need of special knowledge and extensive computational demands of detailed simulations (Rasheed et al. 2020). This acceleration has been fueled by the steady growth in computational power paired with the refined capabilities of AI algorithms (Wang et al. 2020). Building upon the optimization framework, the objective of this surrogate model *(SMUP)* is to rapidly identify an unconventional propeller geometry alongside its open water characteristics.

6.1 Workflow

The workflow of *SMUP*, as depicted in Figure 8, employs a dual-stage optimization originating from a vector of four primary inputs and offers an unconventional propeller design. This yields two results: a vector detailing the design variables and another capturing the open water characteristics, augmented with cavitation estimations. Subsequently, this optimized data set is fed into the surrogate model. The target of this surrogate model is to quickly and accurately predict the optimization outcomes from just the four primary inputs, bypassing the extensive simulation phase.

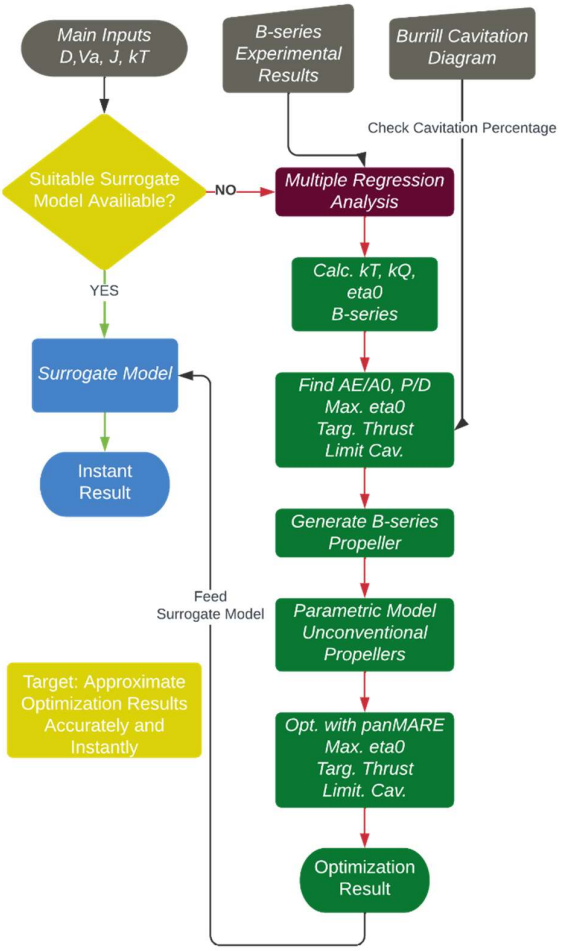

Figure 8: Workflow of Feeding SMUP

6.2 Optimization Data

For the data intake process of the *SMUP*, the *Sobol* sequence (Bratley & Fox 1988) is employed, adeptly exploring the design space by generating 24 input vectors. The adoption of the *Sobol* algorithm is paramount to ensure that *SMUP* functions efficiently across various inputs. Figure 9 depicts a set of four bar charts, with the x-axis representing the index numbers of 24 design instances. In all the graphs, the parameters have been normalized to a range of 0 to 1, allowing for a visual comparison of parameter values. The first graph displays the non-dimensional values of the four primary inputs of the surrogate model, demonstrating how the *Sobol* sequence effectively explores the design space. Subsequently, the B-series optimization is employed to identify the most efficient propeller while targeting a required thrust and limiting cavitation. The propeller geometry is defined by the expanded area ratio and the pitch ratio. It is noteworthy that the optimized outputs from the B-series optimization

closely align with the starting point, indicating its viability. In the third graph, propeller efficiency for the conventional propeller is illustrated, revealing the enhanced performance of the tip rake design for each design instance. On average, the enhanced performance from the optimal unconventional design amounts to approximately 3.3% and the generated thrust exceeds the required amount by around 12%. The final chart displays seven design variables for the parametric model, with bars stacked vertically. These variables exhibit a tendency toward similar designs, such as backward rake and tip rake propellers, similarly to Kappel propellers (Andersen et al. 2005). However, other parameters that influence the chord and the pitch do not exhibit a consistent pattern, likely due to their initial selection in the conventional B-series propeller. Notably, there is an exception: the *scaleChord* parameter suggests that propellers with low chord values can be highly effective in this setup, which is reasonable given that it is an open-water test. Overall, it appears that modifications to the skew curve are not preferable in this setup, as the B-series propeller already possesses a favorable skew curve.

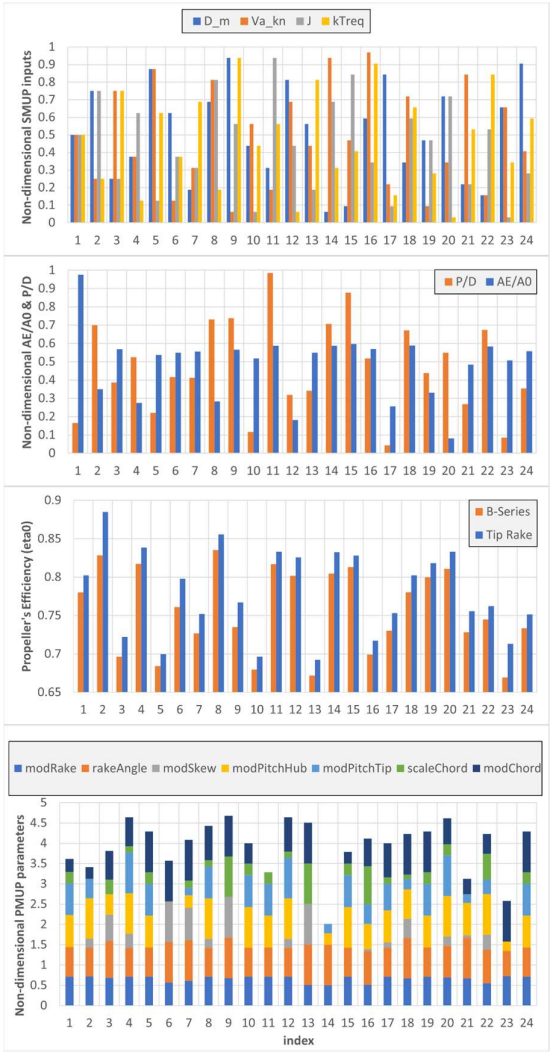

Figure 9: Inputs & Optimization Data from Sobol Sequence for the Development of SMUP

6.3 Feeding the Surrogate Model

Each set of input parameters corresponds to a unique output vector and these output vectors are linked to various aspects of the propeller design process. They encompass the B-series parameters, which are crucial for conventional B-series propeller efficiency, as well as the open-water performance characteristics of the optimal propeller and the design variables specific of the parametric propeller model. The combination of these design variables with the B-series parameters forms the basis for achieving the optimal propeller design for the given input vector through the application of the parametric model. Subsequently, these output vectors are processed by a response surface algorithm within *DAKOTA* (Giunta et al. 2006), which is also integrated into *CAESES*. The response surface algorithm employs various optimization techniques to fine-tune the design based on the input parameters, ensuring that the final propeller design aligns with the desired criteria and the performance objectives. Notably, a common practice in response surface optimization suggests an initial sample size of at least 5 times the number of design variables. In the context of the surrogate model, which consists of four main input variables, aligning with this general guideline leads to the selection of 24 input vectors, thereby ensuring the reliable results.

6.4 Drawbacks on the Surrogate Model

In general, distinctions in propeller geometries become noticeable primarily for vectors within the input domain that differ significantly from the data used in the surrogate model. For example, when seeking the conventional design for the B-series, the surrogate model effectively operates with just two parameters. Concerns arise regarding the inclusion of the rake angle as a design variable for the parametric propeller model, as this addition could potentially lead to substantial changes in propeller shapes. Even minor numerical variations may result in significant deviations in physical form, leading to possible instability. Furthermore, there exists a notable discrepancy between the predicted open water characteristics from the surrogate model and the anticipated outcomes from the optimization. Instances occur where the predicted optimal design violates the required thrust constraint. These concerns emphasize the necessity for a more comprehensive investigation and refinement of the *SMUP*.

7 DISCUSSION

In this section, a comprehensive discussion unfolds, structured into two distinct subsections: one for summarizing conclusions and the other for outlining upcoming future steps of this research.

7.1 Conclusions

In conclusion, the methodological approach of this surrogate model finds its origins in Simulation-Driven Design. While many traditional optimization processes are often more straightforward, the essence of surrogate modeling is simply utilizing optimization data. Once this model accumulates sufficient data, it enables the bypassing of the simulation stage, leading to a substantial

simplification of the design process and time savings. This approach shares similarities with parametric modeling, where the development phase may be more time-intensive compared to simple modeling, yet it offers a broader spectrum of options. Essentially, while individual optimizations may be quicker to set up, the creation of a surrogate model expands the range of potential applications. The innovation of the project lies in its capacity to utilize historical data, including elements like the polynomials of the B-series and the Burril Diagram, which enhance the flexibility and the adaptability of the model. Nonetheless, it is important to note that this surrogate model is still evolving and maturing, given the inherent trial-and-error nature of the process.

7.2 Future Steps

Two primary approaches can be taken to enhance the robustness and the effectiveness of the *SMUP*. Firstly, consider expanding the dataset used by the model with additional optimization data. Secondly, reduce noise in the data by constraining the design space with fewer design variables for the *PMUP*. Moreover, future directions for this research encompass expanding the scope of the surrogate models to account for 3-bladed and 4-bladed propellers, in addition to the 5-bladed designs, as these configurations are among the most common choices in ship propulsion. Also, instead of relying solely on the B-series profile, the incorporation of the NACA 66 profile, a common feature in the propulsion industry, could be explored (Brockett 1966). This approach, coupled with a few design variables for profile manipulation, serves to expand the design space even further. An additional forthcoming step involves integrating a wake field derived from the hull of the ship, replicating the conditions encountered by the propeller, with the aim of further enhancing result accuracy and their direct applicability to real-world scenarios. Notably, the *panMARE* code provides a user-friendly and efficient means of incorporating a wake field into hydrodynamic simulations, rendering it a suitable tool for future developments. Another anticipated development is the creation of a web-app as introduced in Harries et al. (2018) and Hauschulz et al. (2022), analogous to the B-series propeller generator, see *https://www.wageningen-b-series-propeller.com/* and (Hauschulz & Harries 2023). This would empower users to design efficiently via a browser interface, allowing them to input desired parameters and instantly receive an efficient, unconventional propeller design complete with its open water characteristics. Within this web-app, *CAD* operations would be processed on the servers of *FRIENDSHIP SYSTEMS AG*, ensuring that the surrogate model is primed to accurately discern the potential values based on user inputs.

ACKNOWLEMENTS

Parts of the work presented in this paper are co-financed within the R&D project *"DEffProForm"* (**D**esigning **Eff**icient Ship **Pro**pellers with Unconventional **Form**) under the official *FKZ* (Förderkennzeichen) 03SX516. This project is funded by Federal Republic of Germany, Federal Ministry for Economic Affairs and Energy on the orders of the German Bundestag. A fundamental component of this study is the *panMARE* code provided by *TUHH*. The invaluable support and collaboration of Martin Scharf and Roland Gosda, members of the *TUHH* team, are instrumental in achieving the advanced results presented, elevating the quality and depth of this research.

REFERENCES

Ahmed, O., Harries, S., Lohse, J., Salecker, S-E. (2023). 'Parametric Modeling, CFD Simulations, DoE and Machine Learning for the Design of a Planing Boat.' In COMPIT 2023. Kloster Drübeck, Germany.

Andersen, P., Friesch, J., Kappel, J. J., Lundegaard, L., & Patience, G. (2005). 'Development of a marine propeller with nonplanar lifting surfaces.' Marine Technology and SNAME News, 42(03), 144-158.

Arapakopoulos, A., Polichshuk, R., Segizbayev, Z., Ospanov, S., Ginnis, A. I., & Kostas, K. V. (2019). 'Parametric models for marine propellers'. Ocean Engineering.

Barnitsas, M. M., Ray, D., & Kinley, P. (1981). 'KT, KQ and Efficiency Curves for the Wageningen B-series Propellers. ' University of Michigan.

Bauer, M., & Abdel-Maksoud, M. (2012). 'A 3-D potential based boundary element method for modelling and simulation of marine propeller flows.' IFAC Proceedings Volumes 45(2): 1179-1184.

Benini, E. (2004). 'Significance of blade element theory in performance prediction of marine propellers.' Ocean Engineering 31(8-9): 957-974.

Birk, L. (2019). 'Fundamentals of Ship Hydrodynamics: Fluid Mechanics, Ship Resistance and Propulsion.' John Wiley & Sons.

Bratley, P., & Fox, B. L. (1988). 'Algorithm 659: Implementing Sobol's quasirandom sequence generator.' ACM Transactions on Mathematical Software (TOMS) 14(1): 88-100.

Brockett, T. (1966). 'Minimum pressure envelopes for modified NACA-66 sections with NACA A=0.8 camber and BuShips type 1 and type 2 sections. ' David Taylor Model Basin Washington DC Hydromechanics Lab.

Burrill, L. C., & Emerson, A. (1963). 'Propeller cavitation: Further tests on 16in. propeller models in the King's College cavitation tunnel.' International Shipbuilding Progress 10(104): 119-131.

Carlton, J. (2018). 'Marine propellers and propulsion.' Butterworth-Heinemann.

Castro, L. F. S., von Zadow, H., & Vesting, F. (2019). 'Tip Geometry Effects on Performance and Erosion for Tip Rake Propellers.' Sixth International Symposium on Marine Propulsors smp'19, Rome, Italy.

Crighton, D. G. (1985). 'The Kutta condition in unsteady flow.' Annual Review of Fluid Mechanics 17(1): 411-445.

Epps, B., Chalfant, J., Kimball, R., Techet, A., Flood, K., & Chryssostomidis, C. (2009). 'OpenProp: An open-source parametric design and analysis tool for propellers.' Proceedings of the 2009 Grand Challenges in Modeling & Simulation Conference 104-111.

Fine, N. E. (1992). 'Nonlinear analysis of cavitating propellers in nonuniform flow. ' Doctoral dissertation, Massachusetts Institute of Technology.

Gerr, D. (1989). 'Propeller handbook.' International Marine Publishing.

Giunta, A. A., McFarland, J. M., Swiler, L. P., & Eldred, M. S. (2006). 'The promise and peril of uncertainty quantification using response surface approximations.' Structures and Infrastructure Engineering: 175-189.

Harries, S., Lorentz, K., Palluch, J., Praefke, E. (2018). 'Appification of Propeller Modeling and Design via CAESES.' In COMPIT 2018.Pavone, Italy.

Harries, S., & Abt, C. (2019). 'CAESES—The HOLISHIP platform for process integration and design optimization.' In A Holistic Approach to Ship Design: Volume 1: Optimisation of Ship Design and Operation for Life Cycle: 247-293.

Harries, S., & Abt, C. (2019). 'Faster turn-around times for the design and optimization of functional surfaces.' Ocean Engineering.

Harries, S. (2020). 'Practical Shape Optimization Using CFD: State-Of-The-Art in Industry and Selected Trends.' In Conference on Computer Applications and Information Technology in the Maritime Industries (COMPIT 2020). Pontignano, Italy.

Hauschulz, S., Harries, S., Thies, F., von Zadow, H. (2022). 'Web-based Microservices for Fast Modeling and Easy Collaboration.' In HIPER 2022 (14th Symposium on High-Performance Marine Vehicles). Cortona, Italy.

Hauschulz, S., & Harries, S. (2023). 'Reduced-Order Modelling for the Preliminary Design of Propellers.' In 5th Symposium on High-Performance Marine Vehicles – "Technologies for the Ship of the Future".

Hess, J. L., & Smith, A. O. (1967). 'Calculation of potential flow about arbitrary bodies.' Progress in Aerospace Sciences 8: 1-138.

Hess, J. L. (1972). 'Calculation of potential flow about arbitrary three-dimensional lifting bodies.'

Hoerner, S.F. (1965). 'Fluid-dynamic Drag: Practical Information on Aerodynamic Drag and Hydrodynamic Resistance. ' Hoerner Fluid Dynamics.

Kerwin, J. E. (1986). 'Marine propellers.' Annual Review of Fluid Mechanics: 367-403.

Kerwin, J. E., Kinnas, S. A., Lee, J.-T. & Shih, W.-Z. (1987). 'A surface panel method for the hydrodynamic analysis of ducted propellers', Transactions of Society of Naval Architects & Marine Engineers 95.

Koziel, S., Ciaurri, D. E., & Leifsson, L. (2011). 'Surrogate-based methods.' In Computational Optimization, Methods and Algorithms (pp. 33-59).

Krasilnikov, V. (2019). 'CFD modeling of hydroacoustic performance of marine propellers: Predicting propeller cavitation. ' In Proceedings of the 22nd Numerical Towing Tank Symposium, Tomar, Portugal (Vol. 29).

Lim, S. S., Kim, T. W., Lee, D. M., Kang, C. G., & Kim, S. Y. (2014). 'Parametric study of propeller boss cap fins for container ships.' International Journal of Naval Architecture and Ocean Engineering: 187-205.

Lungu, A. (2019). 'Scale effects on a tip rake propeller working in open water. ' Journal of Marine Science and Engineering, 7(11), 404.

Man (2023). 'Basic Principles of Ship Propulsion.' Man Energy Solutions.

Mizzi, K., Demirel, Y. K., Banks, C., Turan, O., Kaklis, P., & Atlar, M. (2017). 'Design optimisation of Propeller Boss Cap Fins for enhanced propeller performance.' Applied Ocean Research, 62, 210-222.

Morino, L., & Bernardini, G. (2001). 'Singularities in BIEs for the Laplace equation; Joukowski trailing-edge conjecture revisited.' Engineering Analysis with Boundary Elements: 805-818.

Netzband, S., Schulz, C. W., Göttsche, U., Ferreira González, D., & Abdel-Maksoud, M. (2018). 'A panel method for floating offshore wind turbine simulations with fully integrated aero-and hydrodynamic modelling in time domain.' Ship Technology Research: 123-136.

Newman, J. N. (2018). 'Marine hydrodynamics.' The MIT press.

Oosterveld, M. W. C., & van Oossanen, P. (1975). 'Further computer-analyzed data of the Wageningen B-screw series.' International Shipbuilding Progress, 22(251), 251-262.

Papakonstantinou, T., Grigoropoulos, G., & Papadakis, G. (2019). 'Marine propeller optimization using open-source CFD.' In Sustainable Development and Innovations in Marine Technologies (pp. 252-259). CRC Press.

Piegl, L., & Tiller, W. (1996). 'The NURBS book.' Springer Science & Business Media.

Politis, G. K. (2004). 'Simulation of unsteady motion of a propeller in a fluid including free wake modeling.' Engineering Analysis with Boundary Elements 28(6): 633-653.

Rasheed, A., San, O., & Kvamsdal, T. (2020). 'Digital twin: Values, challenges and enablers from a modeling perspective.' IEEE Access 8: 21980-22012.

Santos, L., Schleicher, S., & Caldas, L. (2017). 'Automation of CAD models to BEM models for

performance based goal-oriented design methods.' Building and Environment: 144-158.

Sherbaz, S. & Duan, Wenyang (2012). 'Propeller efficiency options for green ship.' Proceedings of 2012 9th International Bhurban Conference on Applied Sciences & Technology (IBCAST), Islamabad, Pakistan.

Sosnowski, M., Krzywanski, J., Grabowska, K., & Gnatowska, R. (2018). 'Polyhedral meshing in numerical analysis of conjugate heat transfer.' EPJ Web of Conferences 180: 02096. EDP Sciences.

Suen, J. B., & Kouh, J. S. (1999). 'Genetic algorithms for optimal series propeller design.' WIT Transactions on The Built Environment 45.

Tadros, M., Ventura, M., & Soares, C. G. (2018). 'Surrogate models of the performance and exhaust emissions of marine diesel engines for ship conceptual design.' Maritime Transportation and Harvesting of Sea Resources – Guedes Soares & Teixeira (Eds).

Troost, L. (1951). 'Open water test series with modern propeller forms.' The North East Coast Institution of Engineers and Shipbuilders in Newcastle upon Tyne, UK.

Van Lammeren, W. P. A., & Vossers, G. (1957). 'The seakeeping laboratory of The Netherlands ship model basin'. International Shipbuilding Progress 4.29: 3-23.

Versteeg, H. K., & Malalasekera, W. (2007). 'An Introduction to Computational Fluid Dynamics: The Finite Volume Method.' Pearson Education.

Wang, B., Xie, B., Xuan, J., & Jiao, K. (2020). 'AI-based optimization of PEM fuel cell catalyst layers for maximum power density via data-driven surrogate modeling. ' Energy conversion and management, 205, 112460.

Xiao, H., & Cinnella, P. (2019). 'Quantification of model uncertainty in RANS simulations: A review.' Progress in Aerospace Sciences 108: 1-31.

Yu, L., Greve, M., Druckenbrod, M., & Abdel-Maksoud, M. (2013). 'Numerical analysis of ducted propeller performance under open water test condition.' Journal of Marine Science and Technology.

Zawawi, M. H., Saleha, A., Salwa, A., Hassan, N. H., Zahari, N. M., Ramli, M. Z., & Muda, Z. C. (2018). 'A review: Fundamentals of computational fluid dynamics (CFD).' In AIP conference proceedings (Vol. 2030, No. 1). AIP Publishing.